Carbohydrate Polymers 116 (2015) 307–313

Contents lists available at ScienceDirect

Carbohydrate Polymers

journal homepage: www.elsevier.com/locate/carbpol

Shape memory starch–clay bionanocomposites

Gildas Coativy[a,b,c], Nicolas Gautier[d], Bruno Pontoire[b,c], Alain Buléon[b,c], Denis Lourdin[b,c,*], Eric Leroy[a,c]

[a] LUNAM Université, CNRS, GEPEA, UMR 6144, CRTT, 37, Boulevard de l'Université, 44606 St Nazaire Cedex, France
[b] UR1268 Biopolymères Interactions Assemblages, INRA, F-44300 Nantes, France
[c] Structure Fédérative IBSM, INRA Nantes-Angers, Rue de la Géraudière, BP 71627, 44316 Nantes Cedex 3, France
[d] Institut des Matériaux Jean Rouxel (IMN), Université de Nantes-CNRS, UMR 6502, 2 rue de la Houssinière, BP 32229, 44322 Nantes Cedex, France

ARTICLE INFO

Article history:
Received 17 November 2013
Received in revised form 6 December 2013
Accepted 9 December 2013
Available online 17 December 2013

Keywords:
Shape memory
Starch
Clay
Bionanocomposite
Melt processing

ABSTRACT

1–10% starch/clay bionanocomposites with shape memory properties were obtained by melt processing. X-ray diffraction (XRD) and TEM evidenced the presence of a major fraction of clay tactoids, consisting of 4–5 stacked crystalline layers, with a thickness of 6.8 nm. A significant orientation of the nanoparticles induced by extrusion was also observed. Tensile tests performed above the glass transition of the materials showed that the presence of clay nanoparticles leads to higher elastic modulus and maximum stress, without significant loss in elongation at break which typically reached 100%. Samples submitted to a 50% elongation and cooled below the glass transition showed shape memory behavior. Like unreinforced starch, the bionanocomposites showed complete shape recovery in unconstrained conditions. In mechanically constrained conditions, the maximum recovered stress was significantly improved for the bionanocomposites compared to unreinforced starch, opening promising perspectives for the design of sensors and actuators.

1. Introduction

Thermoplastic starch is a biobased and biodegradable plastic material that can be obtained from the melting of native starch granules extracted from a variety of widely available crops (Halley et al., 2008). Due to the chemical structure of the anhydroglucose repeating unit, the two starch constituting macromolecules (linear amylose and hyperbranched amylopectin) are highly hydrophilic. Starch is therefore subject to water uptake and plasticization by water molecules (Bizot et al., 1997). The estimated high glass transition temperature of dry amorphous starch, close to 315 °C, typically drops to 70 °C, when starch is stored at a relative humidity (RH) of 50%; and even below 25 °C if the RH is close to 100%. As a consequence, at 25 °C, the same amorphous starch matrix can either have a glass like rigid and fragile mechanical behavior, or a rubber like hyperelastic behavior, depending on moisture conditions. Such a high water sensitivity of thermomechanical properties tends to make thermoplastic starch poorly competitive for the replacement of petroleum-based commodity thermoplastics (in applications) such as packaging(s). Even though the use of non-volatile plasticizers, such as glycerol, allows formulating soft materials by a "stabilization" of starch in the rubbery state, the increase of molecular mobility can favor the recrystallization of starch and a progressive embrittlement (Van Soest & Vliegenthart, 1997). On the contrary, the moisture sensitivity of starch may be an advantage for the design of stimuli responsive functional materials. It has been recently shown that amorphous starch obtained by extrusion can acquire shape memory properties when subjected to adequate thermoforming treatment (Véchambre, Chaunier, & Lourdin, 2010). Such treatment involves a first heating of glassy amorphous starch above its glass transition temperature, in order to be able to subject it to a reversible large deformation in the rubbery state. By cooling the deformed material below its glass transition temperature, a glassy rigid temporary shape is then obtained. Such a thermoformed starch material is able to recover its initial shape if it enters the rubbery state, either by heating above its glass transition temperature, or by plasticization by water, thanks to moisture absorption.

The most promising applications of this new biobased material range from smart food products (Chaunier, Véchambre, & Lourdin, 2012) to biomedical devices since starch is edible and biocompatible. Nevertheless, the mechanical performances of starch in the rubbery state, which determine the ability to recover its shape in a constrained environment, limit the possibilities of using it as a stimuli-responsive actuator (Véchambre, Buleon, Chaunier, Gauthier, & Lourdin, 2011).

* Corresponding author at: UR1268 Biopolymères Interactions Assemblages, INRA, F-44300 Nantes, France.
E-mail addresses: gildas.coativy@univ-nantes.fr (G. Coativy), nicolas.gautier@cnrs-imn.fr (N. Gautier), bruno.pontoire@nantes.inra.fr (B. Pontoire), alain.buleon@nantes.inra.fr (A. Buléon), denis.lourdin@nantes.inra.fr (D. Lourdin), eric.leroy@univ-nantes.fr (E. Leroy).

0144-8617/$ – see front matter © 2013 Elsevier Ltd. All rights reserved.
http://dx.doi.org/10.1016/j.carbpol.2013.12.024

Table 1
Composition of the extruded powder blends, average torque values during melt recirculation and calculated SME values.

Sample	Starch (%)	Water (%)	MMT (%)	SME (J/g)	Torque (N cm)
Starch	70	30	0.0	850 ± 100	98 ± 10
1% MMT	69.9	29.5	0.6	920 ± 100	112 ± 10
3% MMT	68.5	29.5	2.0	1200 ± 100	138 ± 10
5% MMT	67.3	29.5	3.2	1100 ± 100	130 ± 10
10% MMT	63.9	29.7	6.4	1050 ± 100	130 ± 10

One approach for overcoming such limitations is the introduction of clay nanoparticles to reinforce the material, which gave successful results in the case of shape memory polyurethane (Xu et al., 2010). In the present paper, we describe for the first time the elaboration and characterization of shape memory (starch/sodium montmorillonites) bionanocomposites by melt processing in presence of water, without additional plasticizer. We particularly studied the crystalline structure, the dispersion and the orientation of the clay tactoids and individual platelets, in the amorphous starch matrix, and their influence on large deformation mechanical behavior above the glass transition temperature and shape memory properties.

2. Experimental

2.1. Materials and formulations

Potato starch was purchased from Roquette frères (Lestrem, France) and sodium montmorillonites (MMT) from Sigma Aldrich. MMT powder consists of aggregates of clay tactoids, in which negatively charged monocrystalline platelets of 0.95 nm thickness are stacked, with sodium counter ions between the layers. According to the datasheet of the producer (Nanocor), the MMT have a cation exchange capacity of 1450 μequiv. g^{-1}. The individual clay platelets have a density of 2.6 and in-plane dimensions typically ranging from 100 to 130 nm. Such a structure is highly hygroscopic and subject to swelling in presence of water. The interlayer spacing (d_{001}) can be increased from 0.96 nm in the dry state, up to 2 nm when four layers of water are intercalated between the clay platelets of the tactoids (Norrish, 1954). Since this phenomenon results in limited attractive forces between the crystalline layers, it was used to favor exfoliation during melt processing. Clays were first equilibrated at a water activity of 0.97, leading to a water content of 30% (wet basis (w.b.)) and to a basal spacing d_{001} = 1.6 nm. In parallel, starch was oven dried at 100 °C during 30 min, resulting in a water content of 8% (w.b.). Starch and MMT powders were then blended in a mortar and then rehydrated until reaching a global water content of 30% (w.b.), the day before extrusion. Such a procedure leads to an intimate mixing of powders before melt processing. The different used formulations are listed in Table 1: the weight contents of MMT were chosen to obtain bionanocomposites containing 1, 3, 5 and 10% of inorganic matter (dry basis (d.b.)).

2.2. Melt processing and sample preparation

The hydrated powder mixtures were melt-processed with a 7 cm^3 microcompounder (Minilab, Thermo Haake). It is made up of a conical twin screw system with a backflow channel, which can be used as a batch mixing reactor given that the material can be recirculated rather than exiting through the die. Moreover, the conical twin screw system allows simulating the performance of a co-rotating or a counter rotating twin screw extruder. In all operations, the co-rotation operation was applied.

The hydrated powder mixtures were introduced in the microcompounder at 95 °C, with a screw speed of 100 rpm, and recirculated during 10 min before being extruded at lower screw speed (10 rpm). The typical weight of the final extruded rods was 2 g (since the rest of the material stayed into the recirculating area), with a rectangular section of approximately 1 mm × 4 mm.

The torque signal was used to evaluate the specific mixing energy (SME), defined as follows:

$$\mathrm{SME} = \int_0^t \frac{T \cdot 2\pi \cdot n}{M \cdot 60} dt$$

where T is the torque signal at time t, n is the screw speed (rpm) and M is the loaded mass (g).

These experimental conditions allowed a complete disruption of the native starch organization, in conditions combining a high shear rate and a long residence time, in order to obtain an efficient dispersion of the clay. Contrary to the typical extrusion temperature used for potato starch (DellaValle, Boch, Colonna, & Vergne, 1995), generally higher than 120 °C, the use of a temperature below 100 °C, allowed long residence times with low water evaporation during the process, and limited degradation of the macromolecules.

Several batches were produced for each formulation in order to have enough rods for the characterization of both the structure and the thermomechanical behavior of the materials after extrusion, and also for the molding of dogbone tensile test samples for the mechanical tests. In both cases, extruded rods were stored at 57% RH during two weeks before characterization or molding. Thermocompression was performed at 130 °C using a mold sized to the section of the rod in order to avoid any orientation induced by the process. This temperature, significantly higher than the glass transition of the amorphous starch matrix, allowed erasing the thermal history of the samples, which were then stored again at 57% RH during two weeks before mechanical tests.

2.3. Water and clay contents

The amount of clay in extruded samples was checked by thermogravimetric analysis using a TGA 2050 (TA Instruments, DE). About 10 mg of material were heated with a temperature ramp of 10 °C/min under nitrogen atmosphere until 950 °C to destroy the organic part and keep the mineral part of the materials.

The samples were kept at 950 °C during 20 min. The water content of materials (extruded rods or molded tensile test specimens) was assessed by dehydration in an oven at 130 °C during at least 24 h, until an equilibrium constant weight was reached.

2.4. Morphology

Transmission electron microscopy was used to observe the morphology of the bionanocomposites, using an HNAR9000 LaB_6 TEM Microscope (Hitachi), with an accelerating voltage of 300 kV (maximum point to point resolution of 0.18 nm). Samples sections were prepared using a Leica UC7 ultramicrotome equipped with a diamond knife. The ultrathin sections of 100 nm thickness were cut at room temperature and under dry conditions and then transferred onto 300 mesh Cu grids coated with a lacey carbon film.

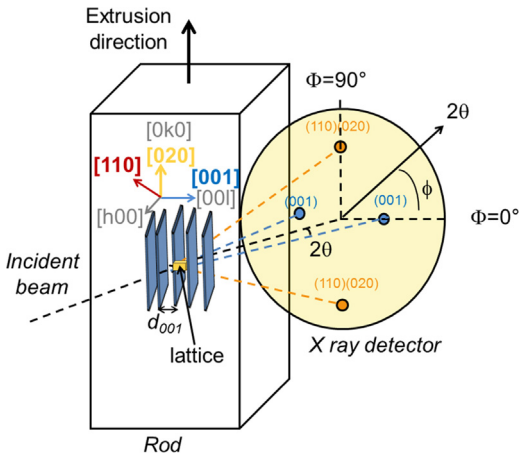

Fig. 1. Experimental X-ray diffraction setup used for the characterization of clay orientation in the bionanocomposites.

2.5. Structural characterizations

X-ray diffraction was used to characterize both extruded rods and samples quenched after being stretched by 50% above their glass transition temperature, using the experimental setting described below. The experimental setup used to study the anisotropic structure of the bionanocomposites samples is illustrated in Fig. 1, in the case of extruded rods. The longitudinal axis of the sample (corresponding to the extrusion flow direction) is perpendicular to the incidental X-ray beam.

Two-dimensional diffraction diagrams were recorded using a Bruker D8 X-ray diffractometer (Karlsruhe, Germany) equipped with a GADDS detector. The X-ray radiation, Cu Kα1 (λ = 0.15406 nm), produced in a sealed tube at 40 kV and 40 mA, was selected and parallelized using crossed Göbel mirrors and collimated to produce a beam 300 or 500 μm in diameter. The sample to detector distance was 8.7 cm and the Bragg angles used ranged from 3° to 26° (2θ).

In order to study the anisotropy of the samples (Fig. 1), the two-dimensional diffraction diagrams were partially integrated along different orientations of the azimuthal angle ϕ: in the case of extruded rods, two directions were considered $\phi = 0°$ and $\phi = 90°$ (as shown in Fig. 1) and the signal was integrated on a ±45° domain around each direction:

$$I_\phi(2\theta) = \int_{\phi-45}^{\phi+45} I(2\theta, \phi)d\phi$$

In that case a limited recording time of 10 min for a beam diameter of 500 μm is allowed obtaining integrated diffraction patterns with acceptable noise levels.

For the tensile test samples elongated above their glass transition, a more detailed analysis was performed, considering five different directions: $\phi = 0°$, $\phi = 30°$, $\phi = 45°$, $\phi = 60°$ and $\phi = 90°$. The signal was integrated on a ±10° domain around each direction:

$$I_\phi(2\theta) = \int_{\phi-10}^{\phi+10} I(2\theta, \phi)d\phi$$

In this second case, the recording time had to be increased to 6 h, in order to obtain a satisfactory signal-to-noise ratio.

Two diffraction peaks are of particular interest to determine the structure and the orientation of clay nanoparticles: the one corresponding to the clay interlayer spacing d_{001}, and the other to crystallographic planes (1 1 0) and (0 2 0) inside clay platelets, whose orientation is orthogonal to the interlayer spacing axis (Bafna, Beaucage, Mirabella, & Mehta, 2003). It is thus possible to evaluate the orientation of clay tactoids by considering these two peaks. In addition, the position of the first peak and the relative intensity of the two peaks provide information about the disruption of the native clay structure. The distance between diffracting planes can be obtained by Bragg's law:

$$2 \times d_{hkl} \times \sin(\theta) = n \times \lambda$$

where θ is the incident angle equal to half the angle corresponding to the maximum of the peak. λ is the wavelength (nm), d is the diffracting distance of the ($h\,k\,l$) plane (nm), and n is the diffracting order.

For an intercalated clay-polymer composite, the peak associated to the interlayer distance d_{001} is shifted to larger distances and therefore lower diffraction angles, compared to native clay. It disappears for a fully exfoliated structure, while the second peak associated to individual platelets should remain.

The average number of stacked clay layers per tactoid may be estimated from the d_{001} peak width, using the Scherrer formula (Jaboyedoff, Kubler, & Thelin, 1999).

$$L = \frac{K \times \lambda}{\Delta 2\theta \times \cos(\theta_0)}$$

where K is a constant (0.89), $\Delta 2\theta$ (rad) is the width at half maximum of the peak, which diffraction angle at the maximum is $2 \times \theta_0$, and λ is the wavelength (0.15406 nm).

L is the coherence length (nm):

$$L = (N - 1) \times d_{001}$$

where N is the number of layers per tactoid.

2.6. Thermal properties

Differential scanning calorimetry (DSC) was used to evaluate the thermal transitions. A Q100 DSC (T.A. Instruments, New Castle, DE) was used, with inox sealed pans, in order to avoid water loss during tests. A first heating from 20 to 95 °C at 3 °C min^{-1} was made to erase the sample history. Then the sample was cooled at 20 °C and heated again to 120 °C at 3 °C min^{-1}. The glass transition temperature (T_g) was evaluated from the thermogram recorded during the second heating ramp, defined as the midpoint of the heat capacity increase.

2.7. Mechanical behavior in the rubbery state

These tests were conducted on thermomolded dogbone specimens using a specially designed system allowing the controlled deformation of the unreinforced starch and starch–clay bionanocomposite samples above their glass transition. Two series of experiments were conducted for each formulation: in a first series of "classical" tensile tests, samples were deformed until break, in order to characterize their mechanical behavior in the rubbery state. In a second series of experiments, the samples were submitted to a maximum elongation limited to 50% and then quenched in this temporary form, in order to characterize the influence of tensile deformation on the nanostructure (see next section) and to assess the shape memory properties.

A tensile test machine Synergie 100 (MTS, Eden Prairie, MN USA) equipped with a 100 N load cell and a specifically designed lower jaw allowing the immersion of the sample in a liquid bath during tensile tests were used. Using a silicone oil bath thermoregulated at 90 °C, it was thus possible to subject the samples (which typically have glass transition temperature close to 70 °C) to large deformations in their rubbery state. The optimized procedure consisted in immersing the sample during 30 s, before the beginning of the tensile test, in order to ensure thermal equilibrium. Force/deformation

curves were recorded for a cross head velocity of 120 mm min^{-1}. Tests were repeated on at least four samples for each formulation.

The strain was defined as the ratio of the displacement of cross head x to the initial length of the sample l_0 (equal to 15 mm).

$$\varepsilon = \frac{x}{l_0}$$

The stress was defined as the ratio of the force F to the initial section of the sample S_0.

$$\sigma = \frac{F}{S_0}$$

The stress–strain curves were analyzed in order to obtain the strain at break (%), the maximum stress (MPa) and the elastic modulus (MPa) determined as the secant modulus at 3% elongation. A minimum of five experimental curves was used to calculate the average values.

2.8. Shape memory assessment

Shape memory was studied both in unconstrained and constrained conditions using the second series of samples (deformed below the breaking strain, fixing an arbitrary elongation of 50%, and quenched). These elongated samples after quenching were first characterized by X-ray diffraction (as described above).

Then, for the assessment of shape memory in unconstrained conditions, samples were stored at 25 °C and at high RH (97%) for two weeks, leading to a decrease of their glass transition temperature, by water sorption and plasticization, down below room temperature. The material thus entered the rubbery state and was able to recover partially or completely its initial shape. The percentage of shape recovery (SR) was taken as the ratio of the recovered strain to the total strain:

$$\text{SR}\ \ (\%) = \frac{L_d - L_r}{L_d - L_i} \times 100$$

where L_i is the initial length, L_d the deformed length and L_r is the recovered length.

Stress recovery in constrained conditions was studied with a DMA 50 (Metravib, Lyon, France), using a temperature ramp from 30 to 150 °C at 3 °C min^{-1}. Sample was coated with hydrophobic grease in order to limit dehydration during the test. Thus the stress recovery can be monitored when the sample reaches the glass-rubbery transition in which the shape memory is stimulated.

3. Results

3.1. Melt processing and characterization of the extruded rods

After melt processing and extrusion, starch rods were transparent indicating efficient thermoplasticization. The starch–clay composites were translucent, with decreasing transparency for increasing clay loading. Fig. 2 shows the typical torque vs time curves obtained during melt processing for the different formulations. The initial increase of the torque during approximately 200 s corresponds to the progressive filling of the microcompounder cavity and melting of the starch matrix. After this step, for all samples, except the one containing 10% of clay, the torque reaches a plateau, with no significant variations during the 600 s fixed recirculation time, thus indicating limited variations of the melt viscosity. For all samples, the sharp decrease at the end of the curves corresponds to the beginning of the melt exit when recirculation is stopped. The average torque values during recirculation and the average calculated specific mechanical energies (SMEs) are reported in Table 1. Taking into account the dispersion of the values, it appears that SME is only slightly influenced by the clay loading, while a more

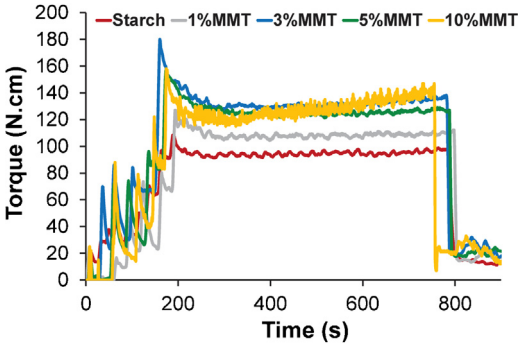

Fig. 2. Torque vs time curves during melt processing of starch and starch–clay compounds.

significant increase of the torque is observed. Compared to the unreinforced starch sample reference, the increased average torque value of the bionanocomposites is due to the presence of clay particles. Nevertheless, no significant variations are observed above 3% clay loading.

3.2. Structure and morphology of the extruded rods

The X-ray diffractograms obtained for the different extruded rods, by integration along azimuthal angles $\phi = 0°$ and $\phi = 90°$, are shown in Fig. 3. For the starch rod, only one curve is shown since no significant differences were observed for the two azimuthal angles. Only a broad amorphous scattering pattern is present, indicating that the starch native crystalline structure has been completely disrupted during melt processing. On the contrary, for the starch–clay composites, diffraction peaks associated to the clay particles can be observed, in addition to the broad scattering of the amorphous starch matrix.

The two characteristic diffraction peaks of MMT are observed for all composites (Fig. 3). The intensity of both peaks strongly increases with clay content. For a 1% clay loading, the intensity is close to the detection limit. The first (peak 1) observed at $2\theta = 5.5°$ corresponds to a clay interlayer spacing distance $d_{001} = 1.6$ nm. Its intensity is always higher for the diffractograms integrated for an azimuthal angle $\phi = 0°$, evidencing a strong orientation of the clay tactoids in the flow direction during extrusion.

Taking into account the thickness of an individual clay platelet (0.95 nm) we obtain a distance between two clay layers equal to 0.65 nm. It is strictly the interlayer distance determined for pure montmorillonite stored at 57% RH, and corresponds to the presence

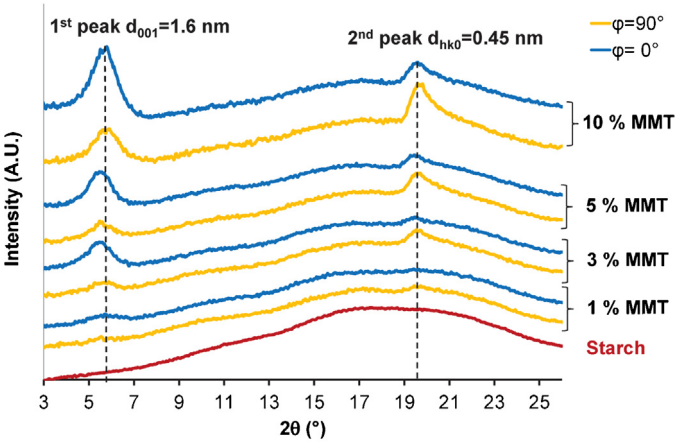

Fig. 3. Integrated diffractograms obtained from the extruded rods, for two azimuthal angles ($\phi = 0°$ and $\phi = 90°$).

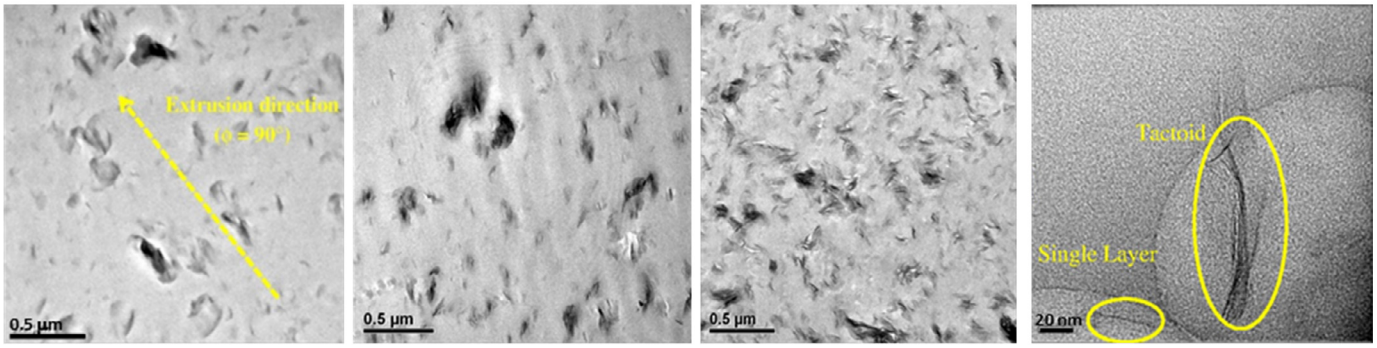

Fig. 4. TEM images of starch–clay bionanocomposites containing 3% of clay (a), 5% of clay (b) and 10% of clay (c) at low magnification (×7000) and of the sample containing 3% clay (d) at higher magnification (×80,000). The extrusion direction is indicated on image (a), as well as examples of particles on image (d).

of two layers of water molecules layers between clay sheets (Huang, Bassett, & Wu, 1994). This value suggests that no intercalated starch macromolecules are present between the clay layers. Nevertheless, the quantitative analysis of the shape of the diffraction peak with the Scherrer formula yields an average tactoid thickness of 6.8 nm. This corresponds to an average number of stacked clay layers per tactoid between 4 and 5.

The second peak present at $2\theta = 19.7^\circ$ is related to the diffracting planes (1 1 0) and (0 2 0) inside a clay platelet. The intensity of this second peak is always higher for diffractograms integrated for an azimuthal angle $\phi = 90^\circ$. This result is consistent with the orientation of the tactoids shown by the first peak, since the diffracting planes (1 1 0) and (0 2 0) are perpendicular to the (0 0 1) planes. Assuming that the tactoids presents into the clay aggregates cannot be oriented, the detected orientation of clay, for all samples, suggests that they are not a lot of aggregates. So the mean population seems to be 6.8 nm sized. Consequently, assuming the usual definition of a bionanocomposite (in which the dispersed particles should have one of their dimensions below 100 nm), one can conclude that starch–clay bionanocomposites were effectively obtained.

Fig. 4a–c presents typical TEM images of starch–clay sections of extruded rods containing 3%, 5% and 10% MMT, respectively. At this magnification (×7000), the clay particles, in black, seem to be well distributed throughout the amorphous starch matrix. Images clearly show that the size of aggregates and the level of aggregation do not increase when clay content increases. This result confirms our assumption based on X-ray experiments, that the quality of the clay dispersion is equal whatever the loading rate (3%, 5% or 10%). The clay particles seem also to be oriented in the direction of extrusion (Fig. 4a), supporting the flow induced anisotropy evidenced by X-ray diffraction. Because of the large section thickness resulting in a low contrast, some layers could be parallel to the cutting plane and therefore not visible. For these reasons, a statistical study of the inter particle distance was not possible. The size of the clay particles apparently shows a large distribution. The thickness of the biggest observed clay aggregates is close to 100 nm.

Images recorded at higher magnification (×80,000), as shown in Fig. 4d for the sample containing 3% clay, confirm the presence of much smaller particles including both individual clay platelets and tactoids with thickness varying from 1 to 10 nm. Similar images were recorded for the other clay contents.

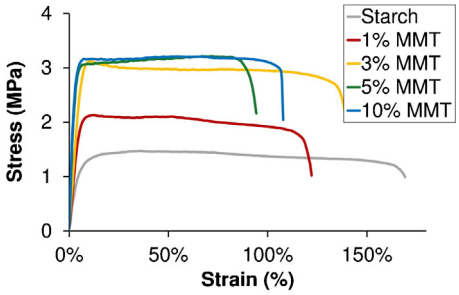

Fig. 5. Typical tensile test curves obtained at 90 °C for starch and starch–clay bionanocomposites.

3.3. Thermal properties of extruded rods

The glass transition temperatures measured during the second temperature ramps of DSC experiments are listed in Table 2. All analyzed samples had almost the same water content (13.7 ± 0.2%), which allows investigating the influence of clay content on the glass transition temperature. The unreinforced starch and the bionanocomposites containing 1–5% clay show one glass transition with very close values of $T_g \approx 72$–74 °C. Conversely, the bionanocomposites containing 10% MMT shows a higher glass transition temperature ($T_g = 80$ °C).

3.4. Tensile tests above the glass transition

Typical stress strain curves obtained for the different formulations at 90 °C are shown in Fig. 5. The average tensile mechanical properties calculated are given in Table 2. All materials display qualitatively the same behavior, below an imposed deformation of about 10%, the stress increases sharply, with an apparent elastic modulus of few tens of MPa. After reaching a stress of a few

Table 2
Water content, glass transition temperatures (T_g), tensile mechanical properties above T_g (at 90 °C) and shape recovery after 50% deformation.

Sample	Water (%)	T_g (°C)	Elastic modulus (MPa)	Maximum stress (MPa)	Strain at break (%)	Unconstrained shape recovery (%)
Starch	13.8	72	32 ± 8	1.5 ± 0.3	138 ± 26	100
1% MMT	13.7	72	45 ± 12	2.3 ± 0.5	111 ± 26	100
3% MMT	13.6	74	62 ± 24	3.1 ± 0.6	115 ± 22	100
5% MMT	13.8	72	83 ± 14	3.9 ± 0.8	87 ± 21	100
10% MMT	13.9	80	84 ± 22	3.1 ± 0.2	119 ± 17	100

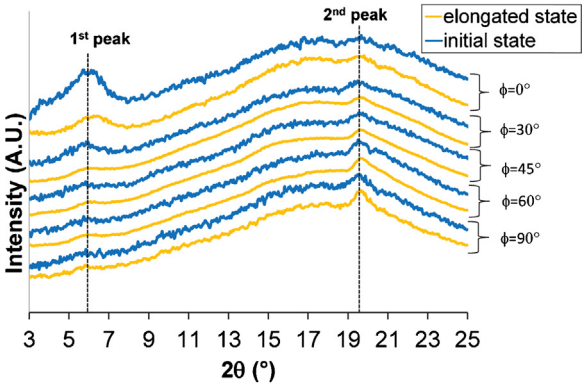

Fig. 6. Integrated diffractograms obtained for tensile test specimens containing 3% of MMT, in initial state and after elongation at 90 °C and quenching (50% strain). Integrations are performed along 5 different azimuthal angles ($\phi = 0°$, 30°, 45°, 60° and 90°).

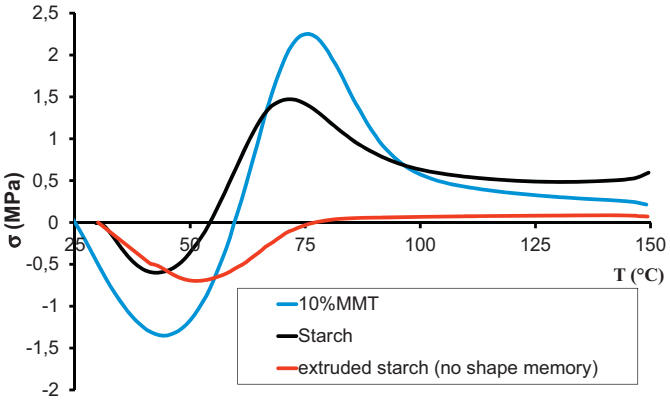

Fig. 7. Stress recovery due to shape memory in mechanically constrained environment (DMA experiment).

MPa (corresponding to the maximum of the curves in Fig. 5, and to the maximum stress values reported in Table 2), the material can be subjected to large deformations before breaking, with no increase of the apparent stress. The calculated average values of the tensile mechanical properties, reported in Table 2 tend to show a non systematic variation of the properties. Nevertheless, taking into account the large dispersion of the measurements, it can be assumed that both the elastic modulus and the maximum stress gradually increase, up to a clay loading of 5%, while, no significant variations seem to occur for higher clay loadings. Besides these variations, the strain at break seems not to be significantly influenced by the presence of clays, for the whole range of concentration studied. Such a trend of mechanical properties has already been observed by other authors for starch/MMT plasticized bionanocomposites (Huang, Yu, & Ma, 2005; Park, Lee, Park, Cho, & Ha, 2003).

3.5. Shape memory samples

As explained in Section 2, a series of samples were elongated by 50% and quenched, in order to assess the shape memory properties.

The X-ray diffractograms recorded for a sample containing 3% clay, before and after elongation are shown in Fig. 6. The intensity of the first peak, corresponding to clay interlayer spacing, clearly decreases for the elongated state, particularly for azimuthal angles of 0° and 30°. No significant intensity change was observed for the second peak, which corresponds to diffraction planes inside clay layers. The decrease of the intensity of the first peak for low azimuthal angles (Fig. 6) could be ascribed to a strain induced delamination of a fraction of the clay tactoids. Further investigations would be necessary to confirm this assumption.

The shape recovery in unconstrained conditions (RH = 97%) was complete for all samples (Table 2). It shows that the presence of clay does not interfere significantly with the shape recovery process of the starch matrix and that the modification of the clay structure in the bionanocomposite in the elongated temporary state does not prevent the shape recovery of bionanocomposites. Unfortunately, it was not possible to perform the same XRD analysis on the samples after shape recovery, due to partial recrystallization of the starch matrix during storage in humid atmosphere.

Fig. 7 illustrates the DMA measurements of stress recovery when shape memory is stimulated in a mechanically constrained environment. In addition the stress evolution obtained for an extruded starch sample (without subsequent 50% elongation at 90 °C and quenching) is shown. For this sample, as temperature is increased, the measured stress decreases first below zero due to thermal expansion and then stabilizes to a value close to zero. On the contrary, for the two other samples, the initial stress decrease (related to thermal expansion) is followed by a strong increase toward a positive value due to shape memory. As the sample cannot recover its shape, a stress is developed, with a maximum value of 1.5 MPa for unreinforced starch and 2.25 MPa for the bionanocomposite.

4. Discussion

The results of melt mixing of natural clay with starch in presence of water allowed obtaining shape memory bionanocomposites with modulated thermo-mechanical properties compared to unreinforced starch. Adding 3–5% clay improves the modulus and maximum strength in the rubbery state, where the shape recovery process takes place, thus opening new perspectives for the development of efficient starch based stimuli responsive actuators. In addition, it was shown that the elongation at break in the rubbery state (here at 90 °C) is not significantly influenced by the presence of clay. This results, which had been observed at room temperature for highly plasticized samples containing glycerol (Park et al., 2003), is particularly important since it potentially allows subjecting the material to large deformations (up to 100% typically) before quenching it in this temporary form.

Moreover, it is the first time that a detailed structural and thermo-mechanical study of melt processed unplasticized (starch/MMT) bionanocomposites with shape memory properties is performed. To our knowledge, the vast majority of the recently reviewed literature on starch–clay bionanocomposites (Vazquez, Cyras, Alvarez, & Moran, 2012) generally deals with the reinforcement of plasticized thermoplastic starch containing large amounts of glycerol and most of the time consisting of composite films obtained by casting from water (Vazquez et al., 2012). Only one single study of extruded (starch/MMT) bionanocomposites was published (Dean, Yu, & Wu, 2007). This study showed the formation of partially exfoliated structures, with a basal spacing of the remaining clay tactoids close to 1.6 nm, as confirmed by our results. Nevertheless, this pioneering work was limited to clay loadings of 3.2% and only showed tensile mechanical properties in the glassy state.

The progressive increase of the tensile mechanical properties for the 1–3% MMT bionanocomposites and the stabilizing for the 5–10% MMT, suggest that no percolating rigid network of particles takes place, contrary to what has been observed for starch/tunicin whiskers bionanocomposites (Angles & Dufresne, 2001).

In the mean time DSC measurements (Table 2) highlights an increase of the glass transition temperature for 10% clay loading, which is shifted about 10 °C toward higher temperatures compared

to unreinforced starch. This could correspond to a slowed down segmental relaxation of macromolecules that are confined between clay nanoparticles. Such a phenomenon has been already observed in many nanocomposites (Fragiadakis, Bokobza, & Pissis, 2011; Kalfus & Jancar, 2007). Depending on the polymer/nanoparticle system, it may lead to restricted (in the case of strong interactions) or enhanced segmental mobility (in the case of repulsive interactions), resulting in increased or decreased glass transition temperatures, respectively (Rittigstein & Torkelson, 2006). In our case, the observed increase of the glass transition temperature is consistent with the presence of a strong affinity between starch and montmorillonites which are both hydrophilic.

The initial objective was to improve the shape memory properties of amorphous starch for sensor–actuators applications, the presence of clay reinforcing nanoparticles increases undoubtedly the maximum recovered stress that starch develops when shape memory is stimulated in a constrained environment (Fig. 7). However, the kinetics of the stress recovery kinetics is modified. The maximum of the stress curve roughly takes place at the glass transition temperatures of the samples. Such a phenomenon will be the subject of future study.

5. Conclusion

Shape memory starch/clay bionanocomposites can be produced without any plasticizers, and a few percent of clay allows their thermomechanical properties to be tuned accordingly to the potential applications considered. Indeed, tensile tests performed above the glass transition of the materials show that the presence of clay nanoparticles leads to higher elastic modulus and maximum stress, without significant loss in elongation at break. The increase of the glass transition temperature for high clay loadings leads to hypothesize the confinement of starch molecules. Concurrently, the high shape recovery ability of amorphous starch is totally preserved for bionanocomposites, with an increase of the recovered stress when the samples are in a mechanically constrained environment opening promising perspectives for the design of sensors and actuators. The bionanocomposites have been obtained by melt processing, using a lab scale process very close to twin-screw extrusion which shows that the production of these materials at an industrial scale is quite possible.

Acknowledgments

The authors would like to gratefully thank the Région des Pays de la Loire and the department INSIS of CNRS, for the Ph.D. Grant attributed to Gildas Coativy. The Région des Pays de la Loire is also acknowledged for supporting the NANOFONC network. The authors also thank Marion De Carvalho for her excellent technical assistance.

References

Angles, M. N., & Dufresne, A. (2001). Plasticized starch/tunicin whiskers nanocomposite materials. 2. Mechanical behavior. *Macromolecules*, *34*, 2921–2931.

Bafna, A., Beaucage, G., Mirabella, F., & Mehta, S. (2003). 3D hierarchical orientation in polymer–clay nanocomposite films. *Polymer*, *44*, 1103–1115.

Bizot, H., LeBail, P., Leroux, B., Davy, J., Roger, P., & Buleon, A. (1997). Calorimetric evaluation of the glass transition in hydrated, linear and branched polyanhydroglucose compounds. *Carbohydrate Polymers*, *32*, 33–50.

Chaunier, L., Véchambre, C., & Lourdin, D. (2012). Starch-based foods presenting shape memory capabilities. *Food Research International*, *47*, 194–196.

Dean, K., Yu, L., & Wu, D. Y. (2007). Preparation and characterization of melt-extruded thermoplastic starch/clay nanocomposites. *Composites Science and Technology*, *67*, 413–421.

DellaValle, G., Boch, Y., Colonna, P., & Vergne, B. (1995). The extrusion behaviour of potato starch. *Carbohydrate Polymers*, *28*, 255–264.

Fragiadakis, D., Bokobza, L., & Pissis, P. (2011). Dynamics near the filler surface in natural rubber-silica nanocomposites. *Polymer*, *52*, 3175–3182.

Halley, P. J., Truss, R. W., Markotsis, M. G., Chaleat, C., Russo, M., Sargent, A. L., et al. (2008). In M. C. Celina, & R. A. Assink (Eds.), *Polymer durability and radiation effects* (pp. 287–300). Oxford (USA): ACS Symposium Series.

Huang, M., Yu, J., & Ma, X. (2005). High mechanical performance MMT-urea and formamide-plasticized thermoplastic cornstarch biodegradable nanocomposites. *Carbohydrate Polymers*, *63*, 393–399.

Huang, W. L., Bassett, W. A., & Wu, T. C. (1994). Dehydration and hydration of montmorillonite at elevated temperatures and pressures monitored using synchrotron radiation. *American Mineralogist*, *79*, 683–691.

Jaboyedoff, M., Kubler, B., & Thelin, P. H. (1999). An empirical Scherrer equation for weakly swelling mixed-layer minerals, especially illite-smectite. *Clay Minerals*, *34*, 601–617.

Kalfus, J., & Jancar, J. (2007). Relaxation processes in PVAc-HA nanocomposites. *Journal of Polymer Science Part B*, *45*, 1380–1388.

Norrish, K. (1954). The swelling of montmorillonite. *Discussions of the Faraday Society*, *18*, 120–134.

Park, H. M., Lee, W. K., Park, C. Y., Cho, W. J., & Ha, C. S. (2003). Environmentally friendly polymer hybrids. Part I. Mechanical, thermal, and barrier properties of thermoplastic starch/clay nanocomposites. *Journal of Materials Science*, *38*, 909–915.

Rittigstein, P., & Torkelson, J. M. (2006). Polymer–nanoparticle interfacial interactions in polymer nanocomposites: Confinement effects on glass transition temperature and suppression of physical aging. *Journal of Polymer Science Part B: Polymer Physics*, *44*, 2935–2943.

Van Soest, J. J., & Vliegenthart, J. F. (1997). Crystallinity in starch plastics: Consequences for material properties. *Trends in Biotechnology*, *15*, 208.

Vazquez, A., Cyras, V. P., Alvarez, V., & Moran, J. (2012). In L. Avérous, & E. Pollet (Eds.), *Environmental silicate nano-biocomposites* (pp. 287–321). London: Springer.

Véchambre, C., Buleon, A., Chaunier, L., Gauthier, C., & Lourdin, D. (2011). Understanding the mechanisms involved in shape memory starch: Macromolecular orientation, stress recovery and molecular mobility. *Macromolecules*, *44*, 9384–9389.

Véchambre, C., Chaunier, L., & Lourdin, D. (2010). Novel shape-memory materials based on potato starch. *Macromolecular Materials and Engineering*, *295*, 115–122.

Xu, B., Fu, Y. Q., Huang, W. M., Pei, Y. T., Chen, Z. G., Jeff, T. M., et al. (2010). Thermal-mechanical properties of polyurethane-clay shape memory polymer nanocomposites. *Polymer*, *2*, 31–39.